DOI: 10.1002/ejic.200500811

# A Single-Source-Precursor Approach to Late Transition Metal Molybdate Materials: The Structural Role of Chelating Ligands in the Formation of Heterometallic Heteroleptic Alkoxide Complexes

**Pia Werndrup,[a] Gulaim A. Seisenbaeva,[a] Gunnar Westin,[b] Ingmar Persson,[a] and Vadim G. Kessler*[a]**

**Keywords:** Cobalt molybdate / EXAFS / Heterogeneous catalysis / Materials / Nickel molybdate / Sol–gel processes

The synthesis and structural determination of three new heterometallic molybdenum complexes, one with cobalt and two with nickel and two of these with β-diketonate ligands and one with amino alcohol ligands, are presented. The reaction of cobalt acetylacetonate with $[MoO(OMe)_4]$ provides $[Co_2Mo_2O_2(acac)_2(OMe)_{10}]$ (**1**) and $[MoO(acac)(OMe)_3]$ (**4**), and the reaction of nickel acetylacetonate with $[MoO(OMe)_4]$ provides $[Ni_2Mo_2O_2(acac)_2(OMe)_{10}]$ (**2**) and **4**. The reaction of $[Ni(OR^N)_2]$ ($R^N$ = $CHMeCH_2NMe_2$) with $[MoO(OMe)_4]$ yields $[Ni_2Mo_2O_2(OR^N)_2(OMe)_{10}]$ (**3**). The two new oxomolybdenum complexes undergo ether elimination upon storage to give the corresponding dioxo complexes $[MoO_2(acac)(OMe)]_2$ (**5**) and $[MoO_2(OR^N)(OMe)]_2$ (**6**). Compounds **3** and **4** could also be obtained from the reaction of stoichiometric amounts of Hacac with $[MoO(OMe)_4]$ and $[MoO_2(OMe)_2]$, respectively. The local structure around the nickel atom in compound **2** in solution and compound **3** in the solid state and in toluene/hexane solution has been determined by means of EXAFS spectroscopy. The complexes are intended to be used as single-source precursors, which are attractive in coatings and for the preparation of mesoporous materials; its application for the synthesis of nickel molybdate by sol–gel processing is therefore reported. The oxide material obtained from **3** displays a uniform grain size and a large surface area. 

## Introduction

The development of low-temperature routes to late transition metal molybdates with small grain size and a high active surface is today one of the most intensively explored fields in materials science related to heterogeneous catalysis. Cobalt and nickel molybdates have been reported to be efficient catalysts in such reactions as oxidative dehydrogenation of alkanes[1] and disproportionation of carbon monoxide with formation of single-walled carbon nanotubes.[2] Nitridation and sulfidation of the initially prepared oxide materials has provided efficient catalysts for higher productivity ammonia synthesis[3] and hydrodesulfurisation reactions,[4] respectively. A great deal of attention has been paid to the properties of the final catalyst in relation to the preparation conditions, especially the pH during the synthesis in aqueous media,[5] and also to the effects of different chemical impurities, both in the original material and introduced by reactants, on the activity and stability of the catalysts.[6] Cobalt and nickel molybdates are usually applied as coatings on different supports, most commonly alumina ($\gamma$-$Al_2O_3$)[6] or activated carbon.[7] Application of these catalysts deposited on niobia for hydrodesulfurisation applications and comparison of the influence of different oxide substrates has been reported.[8] A common approach to late transition metal molybdates is a high-temperature decomposition of a salt mixture, such as $Co(NO_3)_2{\cdot}6H_2O$ and $(NH_4)_6Mo_7O_{24}$, leading to the formation of a molybdate powder.[7,9] Great efforts have been made to enhance homogenisation of the components in the course of preparation of these materials by using approaches such as freeze-drying,[10] impregnation of porous supports by water solutions of salts stabilized by chelating ligands, such as, for example, nitrilotriacetates[11] or ethylenediamine in combination with hydrothermal treatment,[12] and electrodeposition in sulfate-citrate medium.[13] Very recently, a special focus in this research field has been the development of sol–gel approaches to this class of materials, applying silica[14] or non-ionic[15] or block-copolymer zwitterionic surfactants[16,17] to ensure the chemical homogeneity and development of desired morphological features. It would be advantageous to be able to deposit a $M^{II}MoO_4$ phase selectively on substrates from solutions. Single-source precursors have been very successfully used in coatings and the preparation of mesoporous materials. It is very simple, once the precursor has beens prepared, to use sol–gel techniques for spin- or dip-coating of surfaces or to hydrolyse and condense the precursors in

[a] Department of Chemistry, SLU,
P. O. Box 7015, 750 07 Uppsala, Sweden
E-mail: Vadim.Kessler@kemi.slu.se
[b] Department of Materials Chemistry, Ångström Laboratory, Uppsala University,
Box 538, 75121 Uppsala, Sweden
Supporting information for this article is available on the WWW under http://www.eurjic.org or from the author.

  

the solution in order to make a gel, which will become a mesoporous powder after calcination, often at a lower temperature than that used in solid-state reactions.[18] This mesoporous coating will be formed on a chosen substrate, which represents an additional advantage for this procedure.

Heterometallic alkoxide complexes of late and heavy transition metals are of interest as single-source precursors for catalytically active materials. The synthetic approaches to heterometallic compounds are restricted, however, because alkoxides of late transition metals are insoluble and unreactive. A promising pathway to heterometallic complexes is provided by the reaction between a metal alkoxide and a β-diketonate complex of another metal atom. This approach has been pioneered by Mosset et al., who observed formation of cobalt-zirconium[19] and iron-zirconium[20] alkoxide complexes in minor yields in alcoholic media. We have previously[21,22] investigated in detail the interaction of divalent metal β-diketonate complexes and tantalum or niobium alkoxides. The main products of this reaction − a new class of heterometallic heteroleptic alkoxide complexes $[M^{II}_2M^{V}_2(acac)_2(OR)_{12}]$ ($M^{II}$ = Co, Ni, Zn, Mg, R = Me, Et, and $M^{V}$ = Ta, Nb) − are formed quantitatively in hydrocarbon solvents according to Equation (1).

$$[M^{II}(acac)_2] + 2[M^{V}(OR)_5] \rightarrow \tfrac{1}{2}[M^{II}_2M^{V}_2(acac)_2(OR)_{12}] + [M^{V}(acac)(OR)_4 \quad (1)$$

If the late transition metal complex contains a different chelating ligand, the reaction with an alkoxide can provide heterometallic heteroleptic alkoxide complexes with different solubility and reactivity than the homoleptic alkoxide. This will alter the hydrolytic properties and provide a tool to control the sol–gel preparation of materials for catalysis. We present here the synthesis, structure determination and sol–gel processing of three new heterometallic molybdenum complexes, one with cobalt and two with nickel, and two of these with β-diketonate ligands and one with amino alcohol ligands.

## Results and Discussion

### Synthesis of Precursor Compounds

In order to develop the concept of molecular structure design for a synthetic approach to single-source precursors suitable for production of inorganic materials[23] we wanted to use the synthetic strategy formulated with the syntheses of the heterometallic heteroleptic complexes $[M^{II}_2M^{V}_2(acac)_2(OMe)_{12}]$ ($M^{II}$ = Co, Ni, Zn, Mg, and $M^{V}$ = Ta, Nb).[21] These reactions use the β-diketonate metal complexes to provide stability in the solution (due to the chelating effects of the β-diketonate ligands) and the methoxide complexes as Lewis bases. The complexes are formed when the initial $M^{II}/M^{V}$ ratio is lower than 1:2; we tested ratios between 1:2.1 and 1:3.5 and the syntheses were successful. Extending the synthetic strategy to molybdenum and late transition metal complexes, we used cobalt acetylacetonate in the reaction with molybdenum oxomethoxide $[MoO(OMe)_4]$. The reaction was successful and provided $[Co_2Mo_2O_2(acac)_2(OMe)_{10}]$ (**1**) [Figure 1 and Equation (2)] in high yields at Co/Mo ratios less than or equal to 1:2.

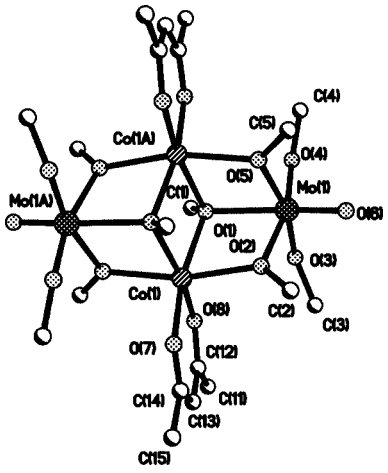


Figure 1. Molecular structure of $[Co_2Mo_2O_2(acac)_2(OMe)_{10}]$ (**1**).

$$[Co(acac)_2] + 2[MoO(OMe)_4] \rightarrow \tfrac{1}{2}[Co_2Mo_2O_2(acac)_2(OMe)_{10}]\ (\mathbf{1}) + [MoO(acac)(OMe)_3]\ (\mathbf{4}) \quad (2)$$

The use of nickel acetylacetonate in hexane instead of cobalt acetylacetonate in the reaction with $[MoO(OMe)_4]$ provided $[Ni_2Mo_2O_2(acac)_2(OMe)_{10}]$ (**2**). The compositions of the reaction products indicate the same reaction pathway [Equation (2)] for both nickel and cobalt acac derivatives, analogous to the one observed earlier for the formation of bimetallic complexes of niobium and tantalum[21,22] [Equation (1)]. Both new cobalt-molybdenum and nickel-molybdenum complexes have much lower solubility in toluene than the corresponding tantalum or niobium ones. In order to improve this low solubility we altered the reaction pathway [Equation (3)] by using an amino alcohol complex, in hexane, instead of the acetylacetonate one.

The use of $Ni(OR^N)_2$ ($R^N$ = $CHMeCH_2NMe_2$) in the reaction with $[MoO(OMe)_4]$ provided the nickel-molybdenum complex $[Ni_2Mo_2O_2(OR^N)_2(OMe)_{10}]$ (**3**). A ligand-exchange reaction occurs when $Ni(L)_2$ (L = acac or $OR^N$) and $[MoO(OMe)_4]$ react in hexane, which gives two new heterometallic heteroleptic alkoxide complexes (**2**, **3**) along with new molybdenum complexes containing the chelating ligand [Equation (3)]. The structure of the by-product com-

$$\begin{array}{l} Ni(L)_2 + 2\ MoO(OMe)_4 \rightarrow \tfrac{1}{2}\ Ni_2Mo_2O_2(L)_2(OMe)_{10}\ (L = acac\ \mathbf{2},\ OR^N\ \mathbf{3}) + MoO(L)(OMe)_3\ (L = acac\ \mathbf{4}) \\ \qquad\qquad\qquad\qquad\qquad\qquad\qquad\qquad \downarrow - Me_2O \\ \qquad\qquad\qquad\qquad\qquad\qquad\qquad\qquad \tfrac{1}{2}\ [MoO_2(L)(OMe)]_2\ (L = acac\ \mathbf{5},\ OR^N\ \mathbf{6}) \end{array} \quad (3)$$

  

plex containing the acac ligand [MoO(acac)$(OMe)_3$] (**4**) (Figure 2, A) was determined by a single-crystal X-ray study. The two new $M^{II}$-molybdenum complexes undergo ether elimination upon storage [Equation (3)] to give the corresponding dioxo complexes [$MoO_2$(acac)$(OMe)]_2$ (**5**) and [$MoO_2(OR^N)(OMe)]_2$ (**6**). The structures of **5** and **6** were also determined by single-crystal X-ray diffraction studies [Figures 2, B and C, respectively]. The presence of dimethyl ether was detected in both mother liquors by the GC-MS technique. Compound **4** was also successfully prepared by the reaction between [$MoO(OMe)_4$] and Hacac. Compound **5** is formed from **4** very slowly at room temperature. An attempt to accelerate this process by refluxing the solutions of **4** led to quick development of a reddish-brown colour associated with reduction of $Mo^{VI}$ to $Mo^{V}$. The mother liquor in this case contained the dimethyl acetal of formaldehyde [$CH_2(OMe)_2$], which is the organic by-product of this reduction reaction.[24] The same kind of reduction associated with ligand redistribution turned out to be major obstacle in the synthesis of **5**, and especially **6**, by the reaction of insoluble [$MoO_2(OMe)_2$] with acetylacetone or (dimethylamino)propanol. The white [$MoO_2(OMe)_2$] turns blue on refluxing with these reagents in toluene, while the solution becomes reddish brown. GC-MS indicated that the solution contained $CH_2(OMe)_2$ in both cases. Compound **5** was isolated in minor yield from the mother liquor by crystallisation, but the solution derived from molybdenum dioxomethoxide and (dimethylamino)propanol did not provide any isolable product.

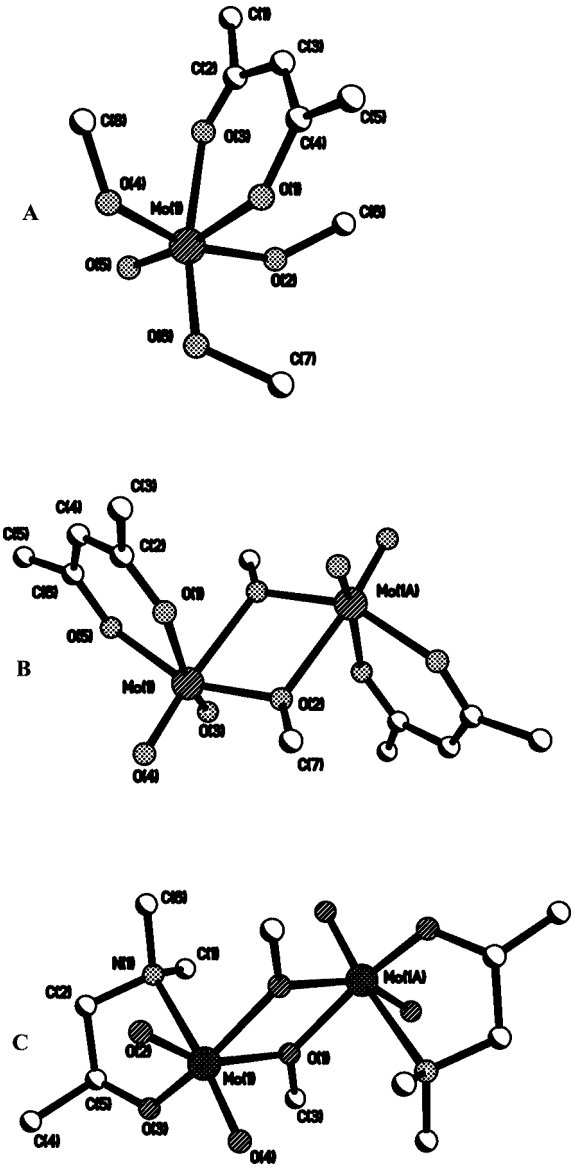


Figure 2. Molecular structure of [MoO(acac)$(OMe)_3$] (**4**; A), [$MoO_2$(acac)$(OMe)]_2$ (**5**; B) and [$MoO_2(OR^N)(OMe)]_2$ (**6**; C).

## Structure Determinations

The molecular structure of the cobalt-molybdenum complex **1** follows the well-known [$Ti_4(OMe)_{16}$] structural type.[25] The structure of **1** was determined by a single-crystal X-ray study (Figure 1 and Table 1). The octahedron surrounding the Co atoms is distorted because of the two types of oxygen atoms from the μ- and $\mu_3$-OR groups in the complex; the *trans* O–Co–O angles are 165.74(14)–166.81(14)°. The acac ring does not distort the octahedron − the O–Co–O angle in the ring is 90.61(16)°. The Co–O distances in **1** are 2.019(4)–2.135(3) Å, depending on the bonding mode of the oxygen atoms. The ionic radii of the cobalt(II) (high spin) and nickel ions in octahedral configuration are 0.745 and 0.690 Å, respectively,[26] and, along with the radius of the water-oxygen-bound di- and trivalent metal ion (1.34 Å),[27] this gives expected Co–O and Ni–O bond lengths of 2.09 Å and 2.03 Å, respectively. The shortest Co–O distances in **1** are to the oxygen atoms in the acac ring (both terminal and chelating) and the longest ones are for the $\mu_3$-oxygens in the complex. In **1**, the Co···C distances in the acac ring are calculated to be 2.995(5) and 2.996(5) Å for the two carbon atoms connected to an oxygen atom in the acac ring, and 3.281(5) Å for the one in the centre of the ring. The molybdenum atom has a distorted octahedral coordination environment with six oxygen atoms. None of the *trans* O–Mo–O angles have ideal 180° angles; they vary between 162.00(17) ° and 165.67(16)°. It is the angle between the two Mo-μ-O bonds that distorts the octahedron the most; it is only 85.59(15)°. The Mo–O bonds for the two terminal methoxide groups [1.857(4) and 1.834(4) Å] are in agreement with the corresponding bonds in complexes such as [$Mo(OMe)_6$][28] and [$Mo_2O_2(OMe)_8$],[29] and very close to those in [$Mg_2Mo_2O_2(OMe)_{10}(MeOH)_4$],[30] a close structural analogue of **1**, where they vary between 1.862(4) and 1.909(4) Å. The two Mo–μ-O bonds are longer [1.998(3) and 1.998(4) Å, respectively] and the Mo–$\mu_3$-O bond is even longer [2.187(3) Å] as this kind of bonding, with an atom shared with one or two other atoms, normally results in a significant increase of bond lengths. The Mo=O bond also causes a deviation from a perfect octahedron. The length of the double bond [1.683(4) Å] is in agreement with the length of the same kind of bond in [$MoO(OMe)_4$] [1.672(5) Å].[29] It is interesting to note that **1** is only the

  

second cobalt-molybdenum alkoxide complex reported in the literature after [{$Mo_2$(DAniF)$_3$}$_2$Co(OMe)$_4$] (DAniF = *N*,*N*′-di-*p*-anisylformamidinate).[31,32]

Table 1. Selected bond lengths [Å] and angles [°] for [$Co_2Mo_2O_2$(acac)$_2$(OMe)$_8$] (**1**).[a]

| | |
|---|---|
| Mo(1)–O(6) | 1.683(4) |
| Mo(1)–O(4) | 1.834(4) |
| Mo(1)–O(3) | 1.857(4) |
| Mo(1)–O(2) | 1.988(3) |
| Mo(1)–O(5) | 1.998(4) |
| Mo(1)–O(1) | 2.187(3) |
| Co(1)–O(8) | 2.019(4) |
| Co(1)–O(7) | 2.026(3) |
| Co(1)–O(2) | 2.123(4) |
| Co(1)–O(5)#1 | 2.126(4) |
| Co(1)–O(1)#1 | 2.130(4) |
| Co(1)–O(1) | 2.135(3) |
| O(6)–Mo(1)–O(4) | 103.5(2) |
| O(6)–Mo(1)–O(3) | 100.8(2) |
| O(4)–Mo(1)–O(3) | 92.35(18) |
| O(6)–Mo(1)–O(2) | 91.44(18) |
| O(4)–Mo(1)–O(2) | 164.69(16) |
| O(3)–Mo(1)–O(2) | 88.00(16) |
| O(6)–Mo(1)–O(5) | 92.15(19) |
| O(4)–Mo(1)–O(5) | 90.50(17) |
| O(3)–Mo(1)–O(5) | 165.67(16) |
| O(2)–Mo(1)–O(5) | 85.59(15) |
| O(6)–Mo(1)–O(1) | 162.00(17) |
| O(4)–Mo(1)–O(1) | 89.68(15) |
| O(3)–Mo(1)–O(1) | 90.65(15) |
| O(2)–Mo(1)–O(1) | 75.00(12) |
| O(5)–Mo(1)–O(1) | 75.31(14) |
| O(8)–Co(1)–O(7) | 90.61(16) |
| O(8)–Co(1)–O(2) | 97.57(15) |
| O(7)–Co(1)–O(2) | 93.49(14) |
| O(8)–Co(1)–O(5)#1 | 93.26(16) |
| O(7)–Co(1)–O(5)#1 | 94.83(15) |
| O(2)–Co(1)–O(5)#1 | 166.25(15) |
| O(8)–Co(1)–O(1)#1 | 165.74(14) |
| O(7)–Co(1)–O(1)#1 | 96.71(14) |
| O(2)–Co(1)–O(1)#1 | 94.19(14) |
| O(5)#1–Co(1)–O(1)#1 | 73.99(14) |
| O(8)–Co(1)–O(1) | 93.18(14) |
| O(7)–Co(1)–O(1) | 166.81(14) |
| O(2)–Co(1)–O(1) | 73.49(12) |
| O(5)#1–Co(1)–O(1) | 97.56(13) |
| O(1)#1–Co(1)–O(1) | 82.44(13) |

[a] Symmetry transformations used to generate equivalent atoms: #1 –*x*, – *y* + 1, –*z* + 2.

The acac ring in compound **4** (part A in Figure 2 and Table 2) distorts the octahedral surrounding of the Mo atom along with the other four oxygens surrounding the Mo atom. The O–Mo–O angle in the acac ring is 80.5(2)° and influences the other O–Mo–O angles such that all four of the O=Mo–O angles are larger than 90° [they vary between 92.0(6)° and 100.6(3)°]. The *trans* O–Mo–O angles are in the range 162.29(19)–171.1(6)°. The Mo–O bond length for the three terminal methoxide groups is 1.846(15)–1.861(4) Å, in agreement with the lengths of the same kind of bonds in [Mo(OMe)$_6$]. The Mo=O bond is also the shortest one in **4** [1.683(14) Å], and the Mo–O bonds to the oxygen in the acac ring are 2.080(10)–2.182(10) Å.

After ether elimination from the two new $M^{II}$-molybdenum complexes [Equation (3)] two new dioxo complexes

Table 2. Selected bond lengths [Å] and angles [°] for [MoO(OMe)$_3$(acac)] (**4**).

| | |
|---|---|
| Mo(1)–O(5) | 1.683(14) |
| Mo(1)–O(6) | 1.846(15) |
| Mo(1)–O(4) | 1.855(4) |
| Mo(1)–O(2) | 1.861(4) |
| Mo(1)–O(1) | 2.080(12) |
| Mo(1)–O(3) | 2.182(10) |
| O(5)–Mo(1)–O(6) | 100.6(3) |
| O(5)–Mo(1)–O(4) | 96.5(7) |
| O(6)–Mo(1)–O(4) | 96.5(6) |
| O(5)–Mo(1)–O(2) | 96.1(7) |
| O(6)–Mo(1)–O(2) | 93.3(6) |
| O(4)–Mo(1)–O(2) | 162.29(19) |
| O(5)–Mo(1)–O(1) | 171.1(6) |
| O(6)–Mo(1)–O(1) | 87.4(5) |
| O(4)–Mo(1)–O(1) | 78.6(5) |
| O(2)–Mo(1)–O(1) | 87.1(5) |
| O(5)–Mo(1)–O(3) | 92.0(6) |
| O(6)–Mo(1)–O(3) | 166.3(5) |
| O(4)–Mo(1)–O(3) | 87.3(5) |
| O(2)–Mo(1)–O(3) | 79.9(4) |
| O(1)–Mo(1)–O(3) | 80.5(2) |

were isolated. The structures of these complexes – [$MoO_2$(acac)(OMe)]$_2$ (**5**) and [$MoO_2$($OR^N$)(OMe)]$_2$ (**6**) – were determined by single-crystal X-ray diffraction studies (Figures 2, B and C, respectively). The molybdenum atoms all have distorted octahedral surroundings in these two complexes. In **5**, the octahedron contains only oxygen atoms, with *trans* O–Mo–O angles in the range 155.02(12)–163.83(15)° (Table 3). The acac ring distorts the octahedron to give an O–Mo–O angle of 80.02(12)°. The Mo–O bonds in the ring are 2.004(3) and 2.166(3) Å, respectively, in good agreement with the same kind of bond in **4**. As with all Mo=O bonds discussed previously, they are the shortest Mo–O bonds in this complex [1.696(3) and 1.697(3) Å, respectively]. In **6**, the octahedron surrounding the Mo atom is composed of five oxygen atoms and one nitrogen atom. The ring distorts the octahedron such that the *trans* N–Mo–O(4) angle is 167.4(3)° and the two *trans* O–Mo–O angles are 153.2(2)° and 155.1(3)° (Table 4). The N–Mo–O(3) angle in the ring is 72.4(2)° and the (μ-O)–Mo–(μ-O) angle is 67.4(2)°. The Mo=O bonds are also the shortest Mo–O ones in **6**, at 1.688(6) and 1.690(6) Å, respectively, and the longest are the Mo–(μ-O) bonds [2.053(6) and 2.175(5) Å]; the Mo–N bond is 2.485(7) Å. The bonding within the aminoalkoxide ring is considerably different from that in the known complexes of $Mo^{VI}$ with triethanolamine, where the presence of several fused chelating cycles results in considerably shortened Mo–N distance, such as 2.342(6) Å in, for example, [$HMoO_2(OC_2H_4)_3N$].[33]

Single crystals of the heterometallic complexes [$Ni_2Mo_2O_2(L)_2(OMe)_{10}$] (**2** and **3**), large enough for single-crystal X-ray studies, have not yet been isolated. The cobalt and nickel atoms are of similar size, and therefore occupy approximately the same volume in a molecule, with nickel being the smaller one (see above). Cobalt atoms have a higher preference to ideal octahedral angles in the inner sphere than nickel. On the other hand, the distortion of the inner sphere of a nickel atom can be severe, and the O–Ni–

  

Table 3. Selected bond lengths [Å] and angles [°] for $[MoO_2(acac)(OMe)]_2$ (**5**).[a]

| | |
|---|---|
| Mo(1)–O(3) | 1.696(3) |
| Mo(1)–O(4) | 1.697(3) |
| Mo(1)–O(2) | 1.991(3) |
| Mo(1)–O(5) | 2.004(3) |
| Mo(1)–O(1) | 2.166(3) |
| Mo(1)–O(2)#1 | 2.264(3) |
| O(3)–Mo(1)–O(4) | 104.19(18) |
| O(3)–Mo(1)–O(2) | 100.58(15) |
| O(4)–Mo(1)–O(2) | 95.15(15) |
| O(3)–Mo(1)–O(5) | 91.48(15) |
| O(4)–Mo(1)–O(5) | 103.05(16) |
| O(2)–Mo(1)–O(5) | 155.02(12) |
| O(3)–Mo(1)–O(1) | 163.83(15) |
| O(4)–Mo(1)–O(1) | 91.18(16) |
| O(2)–Mo(1)–O(1) | 82.67(12) |
| O(5)–Mo(1)–O(1) | 80.02(12) |
| O(3)–Mo(1)–O(2)#1 | 88.71(14) |
| O(4)–Mo(1)–O(2)#1 | 163.06(14) |
| O(2)–Mo(1)–O(2)#1 | 71.37(13) |
| O(5)–Mo(1)–O(2)#1 | 87.27(12) |
| O(1)–Mo(1)–O(2)#1 | 77.25(12) |

[a] Symmetry transformations used to generate equivalent atoms: #1 $-x, -y + 1, -z$.

Table 4. Selected bond lengths [Å] and angles [°] for $[MoO_2(OR^N)OMe]_2$ (**6**).[a]

| | |
|---|---|
| Mo(1)–O(4) | 1.688(6) |
| Mo(1)–O(2) | 1.690(6) |
| Mo(1)–O(3) | 1.895(6) |
| Mo(1)–O(1)#1 | 2.053(6) |
| Mo(1)–O(1) | 2.175(5) |
| Mo(1)–N(1) | 2.485(7) |
| O(4)–Mo(1)–O(2) | 104.6(3) |
| O(4)–Mo(1)–O(3) | 96.3(3) |
| O(2)–Mo(1)–O(3) | 103.6(3) |
| O(4)–Mo(1)–O(1)#1 | 101.5(3) |
| O(2)–Mo(1)–O(1)#1 | 91.1(3) |
| O(3)–Mo(1)–O(1)#1 | 153.2(2) |
| O(4)–Mo(1)–O(1) | 92.4(3) |
| O(2)–Mo(1)–O(1) | 155.1(3) |
| O(3)–Mo(1)–O(1) | 92.2(2) |
| O(1)#1–Mo(1)–O(1) | 67.4(2) |
| O(4)–Mo(1)–N(1) | 167.4(3) |
| O(2)–Mo(1)–N(1) | 83.8(3) |
| O(3)–Mo(1)–N(1) | 72.4(2) |
| O(1)#1–Mo(1)–N(1) | 87.5(2) |
| O(1)–Mo(1)–N(1) | 82.9(2) |

[a] Symmetry transformations used to generate equivalent atoms: #1 $-x, -y, -z + 1$.

O angles are shifted instead of differentiating the Ni–O bond lengths in the octahedron. Despite this difference in inner-sphere flexibility, we propose the structure of **1** as a model for the description of the nickel-molybdenum complexes **2** and **3**.

A powder of the acac complex **2** was studied by Ni-EXAFS (part A in Figure 3 and Table 5), which gave a mean Ni–O distance of 2.024(2) Å (Figure 4, A). This distance is significantly shorter than the same kind of distances in the model, obtained from the X-ray single-crystal experiment, of the cobalt analogue **1** with a range of 2.123(4)–2.135(3) Å for the Co–(μ-O) and Co–($\mu_3$-O) distances. No Ni···C distances could be determined from the EXAFS experiment. The Ni···Ni distance in **2** is 3.150(11) Å and the Ni···Mo distance is 3.311(2) Å, both in agreement with the observed distances in **1** (3.208 Å for Co···Co and 3.348 Å for Co···Mo) taking into account the smaller ionic radius of nickel.

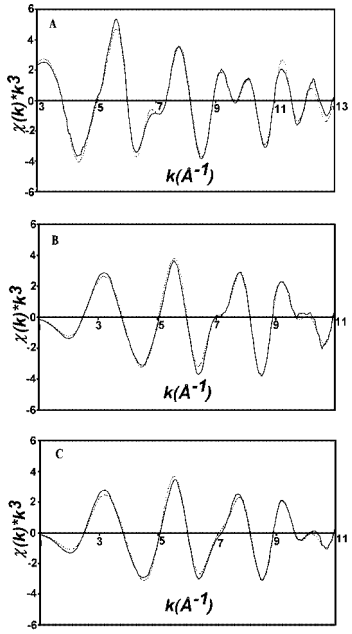


Figure 3. EXAFS spectra of $[Ni_2Mo_2O_2(acac)_2(OMe)_{10}]$ (**2** as a powder; **A**) and $[Ni_2Mo_2O_2(OR^N)_2(OMe)_{10}]$ [**3** as a powder (**B**) and in solution (C)]. Solid lines represent experimental data and dotted lines calculated data.

Table 5. EXAFS model parameters[a] for **2** (in solution) and **3** (powder and in solution).

| Interaction | *N* | *d* [Å] | $\sigma^2$ [Å$^2$] | $E_o$ [eV] | $S_o^2$ |
|---|---|---|---|---|---|
| **2** solution | | | | | |
| Ni–O | 6 | 2.024(2) | 0.0076(2) | 8330.0(3) | 0.83(2) |
| Ni···Ni | 1 | 3.150(11) | 0.015(2) | | |
| Ni···Mo | | 2 | 3.311(2) | 0.0060(1) | |
| **3** powder | | | | | |
| Ni–O | 5 | 2.058(2) | 0.0065(3) | 8329.9(3) | 0.86(3) |
| Ni–N | 1 | 2.336(13) | 0.0088(15) | | |
| Ni···Ni | 1 | 3.144(2) | 0.0040(2) | | |
| Ni···Mo | 2 | 3.297(2) | 0.027(4) | | |
| **3** solution | | | | | |
| Ni–O | 5 | 2.033(3) | 0.0073(6) | 8327.7(4) | 0.69(2) |
| Ni–N | 1 | 2.133(9) | 0.0010(6) | | |
| Ni···Ni | 1 | 3.127(2) | 0.0036(2) | | |
| Ni···Mo | 2 | 3.120(21) | 0.029(4) | | |

[a] The parameters are the number of interactions (*N*), bond length (*d*), Debye–Waller factor ($\sigma^2$), threshold energy ($E_0$) and amplitude reduction factor ($S_0^2$).

A powder and a toluene/hexane solution of **3** were also studied by Ni-EXAFS (B and C in Figures 3 and Table 5). The heterometallic complex is preserved in solution, as can be seen by the similarity of the EXAFS curves. Fourier transforms of the EXAFS curves (Figures 4, B and C) provide similar Ni–O distances in the powder and in solution [2.058(2) Å and 2.033(3) Å, respectively]. The Ni–N bond

  

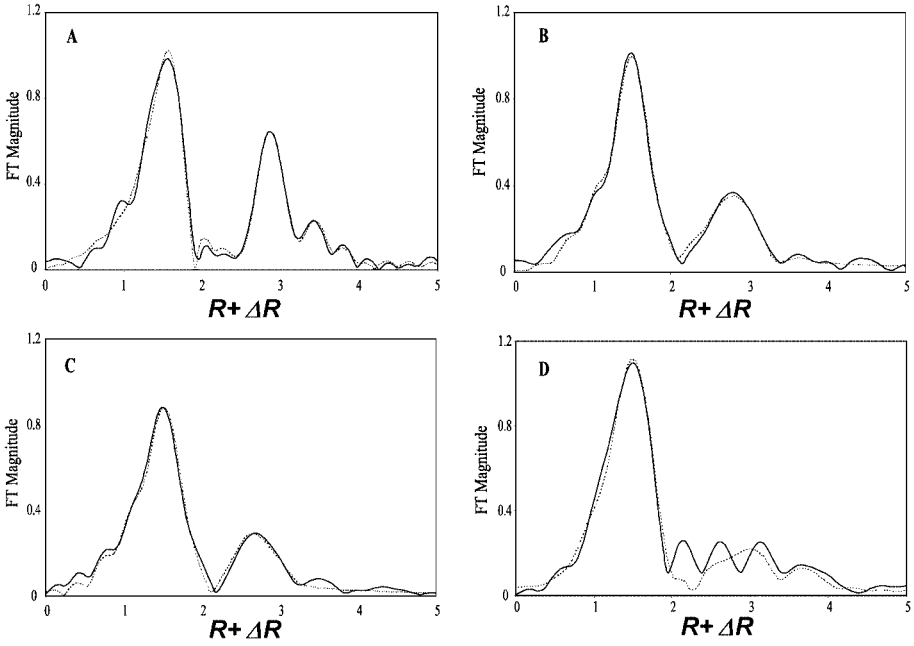


Figure 4. Fourier transforms of $[Ni_2Mo_2O_2(acac)_2(OMe)_{10}]$ (**2** as a powder; **A**), $[Ni_2Mo_2O_2(OR^N)_2(OMe)_{10}]$ [**3** as a powder (**B**) and in solution (**C**)] and $[Co_2Nb_2(acac)_2(OMe)_{12}]$ (powder; D). Solid lines represent experimental data and dotted lines calculated data.

in **3** was determined to be 2.336(13) Å for the powder and 2.133(9) Å for the solution, which is close to the Mo–N bond in **6**. Also for **3** the Ni···Ni distances were refined to 3.144(2) Å for the powder and 3.127(2) Å for the solution. The Ni···Mo distances were refined to 3.297(2) Å for the powder and 3.120(21) Å for the solution, which is in good agreement with the observed distances in **2** and the molecular structure of **1**.

Similarities in the results from the EXAFS experiment of complexes **2** and **3** indicate similarities in the molecular structures of these compounds, the nature of the chelating ligands being the only difference between them. The molecular structures of these heterometallic complexes are therefore analogous and follow the model found in the X-ray single-crystal study well. The Fourier transform of the EXAFS curve for the powder of $[Co_2Nb_2(acac)_2(OMe)_{12}]$ is included for comparison in Figure 4 (see part D).[21] This Co–Nb complex is also a tetranuclear molecule belonging to the $[Ti_4(OMe)_{16}]$ structural type, with Co–O distances of 2.096(11) Å for the four longest bonds and 1.963(14) Å for the two shortest ones, and with Co···Co and Co···Nb distances close to 3.30 Å.

## Sol–Gel Preparation

The sol–gel technique is a useful and attractive means of obtaining nanocomposite materials due to its easy handling

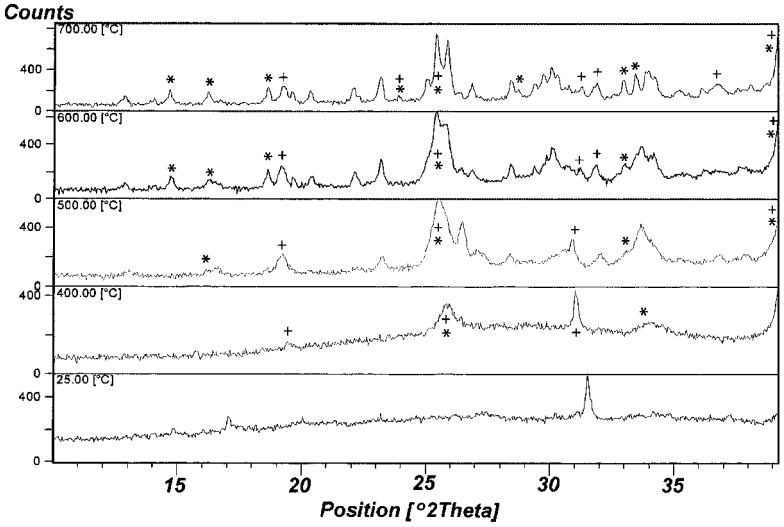


Figure 5. Powder X-ray diffraction of **3** at different temperatures. +: monoclinic (*P*2/*c*) $NiMoO_4$ [16-0291];[34] *: monoclinic (*I*2/*m*) $NiMoO_4$ [33-0948].[34]

  

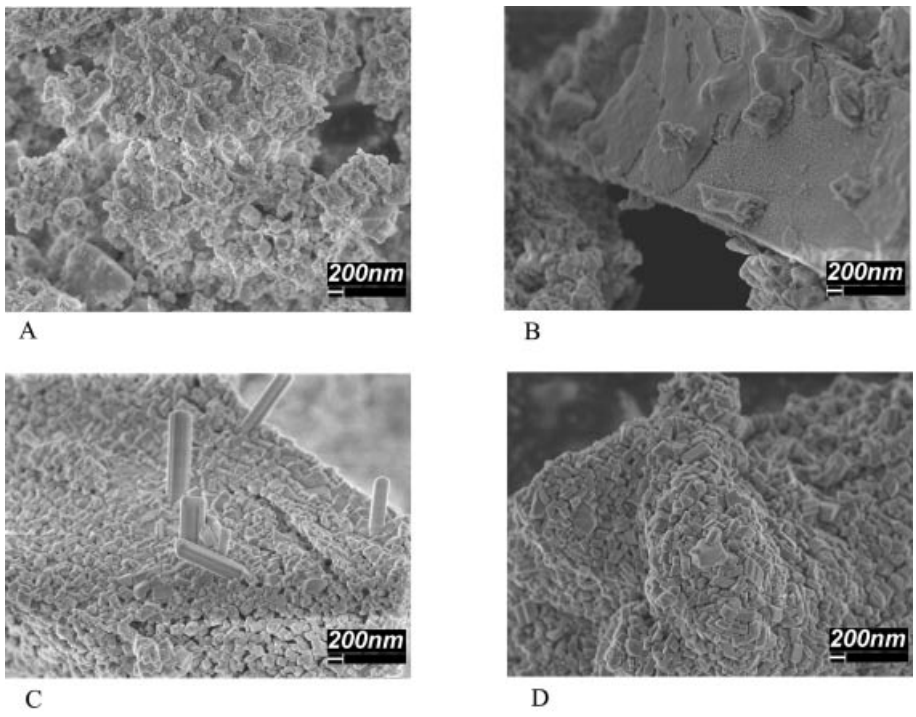


Figure 6. SEM images of the xerogel from **3** annealed at 300 °C (A), 400 °C (B), 500 °C (C) and 700 °C (D).

and low annealing temperatures. Complex **3** was used to obtain xerogel powders. The hydrolysed complex was checked by TGA to confirm the annealing temperatures used. At 315 °C the curve shows a sharp decrease in weight until 420 °C, and at 535 °C the decomposition ends, with only minor weight loss at higher temperatures. Powder X-ray diffraction of the xerogel shows the incipient crystallisation of $NiMoO_4$ [16-0291][34] at 400 °C (Figure 5). At 700 °C, the crystallisation of the monoclinic (*P*2/*c*) oxide $NiMoO_4$ is more pronounced and a monoclinic (*I*2/*m*) $NiMoO_4$ phase [33-0948][34] is seen as well. Scanning electron microscopy of the annealed xerogels confirmed the results from the powder X-ray diffraction analysis. At 300 °C, the gel is porous with a low degree of crystallinity; no sharp edges on the grains can be seen (Figure 6, A). Annealing at 400 °C started the crystallisation and the grains become larger but are still porous (Figure 6, B). The crystallisation process is well underway at 500 °C. The grains are uniform in size (75–100 nm) and well packed with a large surface area (Figure 6, C). Small rods of crystallised oxide can be seen. At 700 °C, the grains are even larger (175–250 nm; Figure 6, D), and rods of crystallised oxide with a diameter of 1 μm are uniformly spread over the sample. The grains have lost the porosity visible at 300 °C, and they are well packed with a large surface area, leaving the material well suited for catalysis experiments.

## Conclusions

The two chelating ligands used appear to play analogous structural roles leading, in both cases studied, to the formation of complexes belonging to the $[Ti_4(OMe)_{16}]$ structural type. The structure of the Co–Mo complex determined by X-ray single-crystal study has been used successfully as a prototype for different Ni–Mo structures studied by EXAFS spectroscopy. The preparation of oxide material from the new nickel-molybdenum amino alcohol complex was successful, with the materials annealed at 500 °C showing uniform grain size and a large surface area.

## Experimental Section

**Reagents and General Procedures:** All experimental procedures were carried out under a dry nitrogen atmosphere using Schlenk techniques or a dry box. $[Ni(OR^N)_2]$ ($R^N$ = $CHMeCH_2NMe_2$), $[MoO(OMe)_4]$ and $[MoO_2(OMe)_2]$ were prepared as described elsewhere.[29,35,36] $[Ni(acac)_2]$ and $[Co(acac)_2]$ (acac = acetylacetonate) (Aldrich, p.a.) were dried by vacuum sublimation.[21] Toluene (Merck, p.a.) and hexane (Merck, p.a.) were dried by distillation over $LiAlH_4$. The IR spectra of nujol mulls were recorded with a Perkin–Elmer FT-IR spectrometer 1720 X. $^1H$ NMR spectra were obtained for solutions in anhydrous $CDCl_3$ with a Bruker 400 MHz spectrometer. SEM was performed with a LEO 1550 high-resolution scanning electron microscope at an accelerating voltage of 20 kV. X-ray powder diffraction was performed with a Phillips SR5056 temperature-programmed diffractometer. Thermogravimetric analysis (TGA) was performed with a Setaram Setsystem 16/18 coupled to a TGA/DSC instrument. The GC-MS analysis was carried out with a JEOL JMS-SX/SX-102A mass spectrometer for fractions of mother liquors distilled in vacuo. The metal ratio in the samples was determined by the Arrhenius Laboratory, Stockholm University, Sweden, with a JEOL-820 scanning electron microscope (SEM) fitted with a Link AN-10000 energy dispersive spectrometer (EDS). The microanalysis data for C, H, N content were obtained at the Laboratory of Organic Analysis at the Moscow State University, Russia, and at MikroKemi AB, Sweden.

  

**Preparation of $[Co_2Mo_2O_2(acac)_2(OMe)_{10}]$ (1):** $[MoO(OMe)_4]$ (1.2477 g, 5.285 mmol) was dissolved in dry toluene (5 mL). $[Co(acac)_2]$ (0.6594 g, 2.567 mmol) was then added (molar ratio Co/Mo = 1:2.1) and the solution was refluxed for 30 min. The solution was cooled and purple crystals of $[Co_2Mo_2O_2(acac)_2(OMe)_{10}]$ (**1**) precipitated at 4 °C overnight. Yield: 1.53 g (1.80 mmol, 70%). $C_{20}H_{44}Co_2Mo_2O_{16}$ (850.29): calcd. C 28.3, H 5.2; found C 27.7, H 4.9. Co/Mo ≈ 1:1 by EDS. IR: $\tilde{\nu}$ = 2932 s cm$^{-1}$, 2857 s, 2726 s, 2672 sh, 2362 w, 2343 w, 2027 br, 1571 s, 1461 s, 1377 s, 1304 s, 1090 s, 970 w, 941 w, 891 w, 847 w, 768 sh, 627 s, 565 br.

**Preparation of $[Ni_2Mo_2O_2(acac)_2(OMe)_{10}]$ (2):** $[MoO(OMe)_4]$ (0.2276 g, 0.964 mmol) was dissolved in dry hexane (6 mL). $[Ni(acac)_2]$ (0.1238 g, 0.482 mmol) was then added (molar ratio Ni/Mo = 1:2) and the solution was refluxed for 30 min. After cooling, dry toluene (1 mL) was added and the solution was refluxed again for 15 min. Small greenish crystals of $[Ni_2Mo_2O_2(acac)_2(OMe)_{10}]$ (**2**) precipitated at 4 °C overnight. Yield: 0.246 g (0.289 mmol, 60%). $C_{20}H_{44}Mo_2Ni_2O_{16}$ (849.80): calcd. C 28.2, H 5.2; found C 27.8, H 5. In 100% metal content Ni = 52.7% and Mo = 47.3% by EDS. IR: $\tilde{\nu}$ = 2921 s cm$^{-1}$, 2726 s, 2672 w, 2363 w, 1576 s, 1518 s, 1456 s, 1376 s, 1307 sh, 1260 sh, 1196 sh, 1151 w, 1088 s, 1044 w, 1016 sh, 987 w, 934 w, 920 w, 897 w, 767 s, 627 s, 553 br. After several weeks at –30 °C crystals of $[MoO(acac)(OMe)_3]$ (**4**) and $[MoO_2(acac)(OMe)]_2$ (**5**) (identified by their single-crystal X-ray unit-cell parameters) were obtained in minor yields from the decanted solution.

**Isolation and Direct Synthesis of $[MoO(acac)(OMe)_3]$ (4) and $[MoO_2(acac)(OMe)]_2$ (5):** $[MoO(acac)(OMe)_3]$ (**4**) was obtained in a practically quantitative yield by addition of a stoichiometric amount of Hacac to $[MoO(OMe)_4]$. Thus, $[MoO(OMe)_4]$ (0.2168 g, 0.918 mmol) was dissolved in hexane (4 mL) at room temperature and Hacac (0.09 mL) was added with a syringe. The slightly brownish-yellow solution was evaporated in vacuo and the brownish-yellow powder obtained was identified as **4** by microanalysis and spectroscopic data (quantitative yields). $C_8H_{16}MoO_6$ (304.15): calcd. C 31.6, H 5.3; found C 30.7, H 5.5. IR: $\tilde{\nu}$ = 1595 br cm$^{-1}$, 1521 s, 1461 s, 1377 s, 1307 w, 1271 s, 1090 s, 941 s, 817 w, 771 w, 656 w, 627 s, 567 br. $^1$H NMR ($CDCl_3$): $\delta$ = 5.75 (1 H, acac-C*H*), 4.71 {3 H, C$H_3$-[O(6)Me]}, 4.41 {6 H, C$H_3$-[O(2 and 4)Me]}, 2.11 [6 H, C$H_3$-(acac-Me)] ppm. $[MoO_2(acac)(OMe)]_2$ (**5**) was obtained in moderate yields (25–30%), although always contaminated with minor amounts of $[MoO_2(acac)_2]$, by treatment of $[MoO_2(OMe)_2]$ with sub-stoichiometric amounts of Hacac in hexane at reflux. In a typical procedure, $[MoO_2(OMe)_2]$ (0.8162 g, 4.3 mmol) was mixed with 5 mL of hexane and Hacac (0.21 mL, 2.1 mmol) and refluxed for 30 min. The light yellow mother liquor was separated by decantation and the solvents evaporated to dryness. The resulting yellowish residue was recrystallised from 1 mL of hexane. Yield: 0.1409 g (26% in relation to Hacac). $C_{12}H_{20}Mo_2O_{10}$ (516.16): calcd. C 27.9, H 3.9; found C 27.6, H 3.8. IR: $\tilde{\nu}$ = 1591 s cm$^{-1}$, 1527 s, 1461 s, 1377 s, 1305 w, 1275 s, 1091 s, 1031 m, 982 s, 931 s, 819 w, 769 sh, 628 s, 565 br. $^1$H NMR ($CDCl_3$): $\delta$ = 5.84 (1 H, acac-C*H*), 3.50 {3 H, C$H_3$-[O(6)Me]}, 2.14 [3 H, C$H_3$-(acac-Me)], 216 [3 H, C$H_3$-(acac-Me)] ppm.

Preparation of both **4** and **5** can also be carried out with toluene as solvent but provides only a few single crystals of these compounds, probably due to their much higher solubility in this solvent. The yields could be increased by subsequent recrystallisation from hexane, but application of the latter for the whole synthetic procedure appears more attractive.

**Preparation of $[Ni_2Mo_2O_2(OR^N)_2(OMe)_{10}]$ (3):** $[MoO(OMe)_4]$ (0.3815 g, 1.616 mmol) was dissolved in dry hexane (4 mL). $[Ni(OR^N)_2]$ (0.2828 g, 0.7963 mmol) was then added (molar ratio Ni/Mo = 1:2) and the solution was refluxed for 30 min. After cooling, dry toluene (1 mL) was added and the solution was refluxed again for 15 min. Small greenish crystals of $[Ni_2Mo_2O_2(OR^N)_2(OMe)_{10}]$ (**3**) precipitated at 4 °C overnight. Yield: 0.375 g (0.438 mmol, 55%). $C_{20}H_{54}Mo_2N_2Ni_2O_{14}$ (855.91): calcd. C 28.0, H 6.3, N 3.3; found C 29.1, H 6.4, N 3.5. In 100% metal content Ni = 55.2% and Mo = 44.8% by EDS. IR: $\tilde{\nu}$ = 3354 br cm$^{-1}$, 3191 sh, 2921 s, 2852 s, 2726 s, 1603 s, 1461 s, 1377 s, 1309 w, 1279 w, 1136 s, 1088 s, 1032 s, 942 s, 902 s, 860 s, 835 s, 722 s, 627 s, 595 s, 532 s, 509 w, 476 w. The decanted solution was stored at –30 °C for several weeks and $[MoO_2(OR^N)(OMe)]_2$ (**6**) precipitated (minor yield).

**X-ray Structure Determinations:** Data collection was performed using a Bruker SMART CCD 1 K diffractometer, at 295(2) K, with Mo-$K_\alpha$ radiation ($\lambda$ = 0.71073 Å; see Table 6 for details). The SAINT PLUS and the SHELXTL-NT program packages were used for data reduction and computations.[37] Empirical absorption correction was applied using the Bruker SADABS program package. The structures were solved by direct methods. The coordinates of the heavy atoms were taken from the initial solution and the non-hydrogen atoms were located in subsequent Fourier syntheses.

Table 6. Crystallographic data for **1**, **4**, **5** and **6**.

| | **1** | **4** | **5** | **6** |
|---|---|---|---|---|
| Identification code | como1m | mooacn1m | mooac1m | nimo220 |
| Empirical formula | $C_{20}H_{44}Co_2Mo_2O_{16}$ | $C_8H_{16}MoO_6$ | $C_{12}H_{20}Mo_2O_{10}$ | $C_{12}H_{30}Mo_2N_2O_8$ |
| Formula weight | 850.29 | 304.15 | 516.16 | 522.26 |
| Space group | $P\bar{1}$ | $P2_1$ | *Pbca* | $P2_1/n$ |
| *a* [Å] | 8.136(4) Å | 7.2455(19) | 8.109(3) | 7.152(4) |
| *b* [Å] | 10.596(6) Å | 12.124(3) | 13.392(5) | 12.154(7) |
| *c* [Å] | 10.951(6) Å | 7.3576(19) | 16.074(5) | 11.240(6) |
| *α* [°] | 112.390(9) | 90 | 90 | 90 |
| *β* [°] | 90.983(10) | 112.922(4) | 90 | 91.959(13) |
| *γ* [°] | 112.259(10) | 90 | 90 | 90 |
| Volume [Å$^3$] | 793.4(7) | 595.3(3) | 1745.6(10) | 976.5(9) |
| *Z* | 1 | 2 | 4 | 2 |
| $d_{calcd.}$ [Mg m$^{-3}$] | 1.780 | 1.697 | 1.964 | 1.776 |
| Absorption coeff. [mm$^{-1}$] | 1.865 | 1.108 | 1.484 | 1.322 |
| Reflections collected | 4070 | 2867 | 10211 | 1357 |
| Independent reflections | 2766 [*R*(int) = 0.0274] | 1922 [*R*(int) = 0.0278] | 2151 [*R*(int) = 0.1431] | 889 [*R*(int) = 0.0281] |
| Final *R* indices [$I > 2\sigma(I)$] | *R*1 = 0.0389, *wR*2 = 0.0816 | *R*1 = 0.0358, *wR*2 = 0.0735 | *R*1 = 0.0412, *wR*2 = 0.0883 | *R*1 = 0.0412, *wR*2 = 0.0983 |
| *R* indices (all data) | *R*1 = 0.0703, *wR*2 = 0.0861 | *R*1 = 0.0503, *wR*2 = 0.0762 | *R*1 = 0.0879, *wR*2 = 0.1021 | *R*1 = 0.0547, *wR*2 = 0.1030 |

  

The structures were refined by full-matrix least-squares techniques in an isotropic and then finally in an anisotropic approximation.

CCDC-283731 to -283734 (for **1**, **4**, **5** and **6**, respectively) contain the supplementary crystallographic data for this paper. These data can be obtained free of charge from The Cambridge Crystallographic Data Centre via www.ccdc.cam.ac.uk/data_request/cif.

**EXAFS Data Collection and Data Treatment:** Nickel and cobalt K-edge X-ray absorption spectra were recorded at the wiggler beam line 4-1 at the Stanford Synchrotron Radiation Laboratory (SSRL), Stanford, USA. SSRL operates at 3.0 GeV and at a maximum current of 100 mA. The EXAFS station was equipped with a Si[220] double crystal monochromator. Data collection was performed in transmission and fluorescence mode simultaneously at ambient temperature. Higher-order harmonics were reduced by detuning the second monochromator to 50% of the maximum intensity at the end of the scans. The solid compounds were diluted with boron nitride to give an edge step of about one unit in the logarithmic intensity ratio, and the sample cells were made of 1-mm brass frames and Mylar tape windows. The toluene/hexane solution was measured in a sample cell with a 2-mm Vitone spacer and Kapton tape windows. The energy scales of the X-ray absorption spectra were calibrated by assigning the first inflection points of the K edges of a nickel foil to 8331.6 eV and a cobalt foil to 7709.5 eV.[38] For each sample 2–3 scans were averaged, giving satisfactory data ($k^3$-weighted) up to $k = 14$ Å$^{-1}$. The EXAFSPAK program package was used for all data treatment and refinement.[39] The EXAFS oscillations were obtained after performing standard procedures for pre-edge subtraction, normalisation and spline removal. The $k^3$-weighted model functions were calculated using ab initio calculated phase and amplitude parameters obtained by the FEFF7 program package (version 7.01).[40] The given errors of the calculated bond lengths in Table 5 originate from the EXAFSPAK algorithms. The errors given are the statistical ones and the true errors of the bond lengths are usually a few times larger.

**Hydrolysis and Heat-Treatment:** Hydrolysis of **3** was performed in toluene by adding an equimolar amount of water with respect to the number of alkoxy groups in **3** and stirring. The sol was poured into a dish and the solvent evaporated to leave a fine powder. The thermal evolution of the powder was investigated by TGA in air at a rate of 10 °C min$^{-1}$ between 23 and 800 °C. Oxide formation of the hydrolysed **3** was performed by heating the powder in air at a rate of 10 °C min$^{-1}$ to the annealing temperature (300–700 °C) for 60 min in a Comecta SA 3L furnace. Scanning electron microscopy (SEM) was performed on the samples in order to study their morphology. X-ray powder diffraction was used to establish the nature of the obtained phases.

**Supporting Information** (see footnote on the first page of this article): $^1$H NMR spectra of [MoO(acac)(OMe)$_3$] (**4**) and [MoO$_2$(acac)(OMe)]$_2$ (**5**) in Figure S1.

## Acknowledgments

Financial support from the Swedish Research Council (VR) is gratefully acknowledged. Mr. Anders Johansson at the Department of Materials Chemistry Ångström Laboratory, Uppsala University, Sweden, is acknowledged for running the SEM analysis. Mr. Gerald Spijksma, Inorganic Materials Science Group, University of Twente, The Netherlands, is acknowledged for help with TGA and XRD analyses. Mr. Rolf Andersson, SLU, is acknowledged for help with the NMR studies. Portions of this research were carried out at the Stanford Synchrotron Radiation Laboratory, a national user facility operated by Stanford University on behalf of the U.S. Department of Energy, Office of Basic Energy Sciences. The SSRL Structural Molecular Biology Program is supported by the Department of Energy, Office of Biological and Environmental Research, and by the National Institutes of Health, National Centre for Research Resources, Biomedical Technology Program.

[1] M. M. Barsan, F. C. Thyrion, *Catal. Today* **2003**, *81*, 159–170.
[2] J. E. Herrera, L. Balzano, A. Borgna, W. E. Alwarez, D. E. Resasco, *J. Catal.* **2001**, *204*, 129–145.
[3] R. Kojima, K. Aika, *Appl. Catal. A* **2001**, *215*, 149–160.
[4] H. Nakamura, M. Amemiya, K. Ishida, *J. Jpn. Petrol. Inst.* **2005**, *48*, 281–289.
[5] M. Barsan, A. Maione, F. C. Thyrion, *Stud. Surf. Sci. Catal.* **2002**, *143*, 1063–1072.
[6] M. N. Kwini, J. M. Botha, *Appl. Catal. A* **2005**, *280*, 199–208.
[7] M. Ferrari, B. Delmon, P. Grange, *Microporous Mesoporous Mater.* **2002**, *56*, 279–290.
[8] A. C. Faro, P. Grange, A. C. B. dos Santos, *Phys. Chem. Chem. Phys.* **2002**, *4*, 2997–4007.
[9] S. A. Halawy, *Monatsh. Chem.* **2003**, *134*, 371–380.
[10] D. Vie, E. Martinez, F. Sapina, J. V. Folgado, A. Beltran, R. X. Valenzuela, V. Cortes-Corberan, *Chem. Mater.* **2004**, *16*, 1697–1703.
[11] A. J. van Dillen, R. J. A. M. Terörde, D. J. Lensveld, J. W. Geus, K. P. de Jong, *J. Catal.* **2003**, *216*, 257–264.
[12] L. A. Palacio, A. Echavarría, S. Sierra, E. A. Lombardo, *Catal. Today* **2005**, *107–108*, 338–345.
[13] E. Gomez, E. Pellicer, E. Valles, *J. Electroanal. Chem.* **2005**, *580*, 222–230.
[14] A. Maione, M. Devillers, *J. Solid State Chem.* **2004**, *177*, 2339–2349.
[15] D. Genuit, P. Afanasiev, M. Vrinat, *J. Catal.* **2005**, *235*, 302–317.
[16] F. Rullens, M. Devillers, A. Laschewsky, *J. Mater. Chem.* **2004**, *14*, 3421–3426.
[17] F. Rullens, N. Deligne, A. Laschewsky, M. Devillers, *J. Mater. Chem.* **2005**, *15*, 1668–1676.
[18] L. G. Hubert-Pfalzgraf, *J. Mater. Chem.* **2004**, *14*, 3113–3123.
[19] R. Schmid, A. Mosset, J. Galy, *Inorg. Chim. Acta* **1991**, *179*, 167–170.
[20] R. Schmid, H. Ahamdane, A. Mosset, *Inorg. Chim. Acta* **1991**, *190*, 237–240.
[21] P. Werndrup, V. G. Kessler, *J. Chem. Soc., Dalton Trans.* **2001**, 574–579.
[22] P. Werndrup, M. Verdenelli, F. Chassagneux, S. Parola, V. G. Kessler, *J. Mater. Chem.* **2004**, *14*, 344–350.
[23] V. G. Kessler, *Chem. Commun.* **2003**, 1213–1222.
[24] V. G. Kessler, K. V. Nikitin, A. I. Belokon', *Polyhedron* **1998**, *17*, 2309–2311.
[25] D. A. Wright, D. A. Williams, *Acta Crystallogr., Sect. B* **1968**, *24*, 1107–1114.
[26] R. D. Shannon, *Acta Crystallogr., Sect. A* **1976**, *32*, 751–767.
[27] J. K. Beattie, S. P. Best, B. W. Skelton, A. H. White, *J. Chem. Soc., Dalton Trans.* **1981**, 2105–2111.
[28] G. A. Seisenbaeva, L. Kloo, P. Werndrup, V. G. Kessler, *Inorg. Chem.* **2001**, *40*, 3815–3818.
[29] V. G. Kessler, A. V. Mironov, N. Y. Turova, A. I. Yanovsky, Y. T. Struchkov, *Polyhedron* **1993**, *12*, 1573–1576.
[30] M. Antipin, Y. Struchkov, A. Shilov, A. Shilova, *Gazz. Chim. Ital.* **1993**, *123*, 265–270.
[31] F. A. Cotton, N. S. Dalal, C. Y. Liu, C. A. Murillo, M. J. North, X. Wang, *J. Am. Chem. Soc.* **2003**, *125*, 12945–12952.
[32] F. A. Cotton, C. Y. Liu, C. A. Murillo, X. Wang, *Inorg. Chem.* **2003**, *42*, 4619–4623.
[33] S. C. Liu, L. D. Ma, D. McGowty, J. Zubieta, *Polyhedron* **1990**, *9*, 1541–1553.

  

[34] JCPDS Powder Diffraction Database, File card number, International Centre for Diffraction Data, Newtown Square, PA, USA, **1997**.
[35] P. Werndrup, S. Gohil, V. G. Kessler, M. Kritikos, L. G. Hubert-Pfalzgraf, *Polyhedron* **2001**, *20*, 2163–2169.
[36] N. Y. Turova, V. G. Kessler, S. I. Kucheiko, *Polyhedron* **1991**, *10*, 2617–2628.
[37] SHELXTL 5.3 Reference Manual, Bruker AXS, Madison, WI, USA, **1997**.
[38] A. Thompson, D. Attwood, E. Gullikson, M. Howells, K.-J. Kim, J. Kirz, J. Kortright, I. Lindau, P. Pianatta, A. Robinson, J. Scofield, J. Underwood, D. Vaughan, G. Williams, H. Winick, *X-ray Data Booklet*, Lawrence Berkeley National Laboratory, **2001**.
[39] G. N. George, I. J. Pickering, *EXAFSPAK − A Suite of Computer Programs for Analysis of X-ray Absorption Spectra* (Eds.: G. N. George, I. J. Pickering), SSRL, Stanford, CA, **1993**.
[40] a) S. I. Zabinsky, J. J. Rehr, A. Ankudinov, R. C. Albers, M. J. Eller, *Phys. Rev. B* **1995**, *52*, 2995–3009; b) A. Ankudinov, Ph. D. Thesis, University of Washington, **1996**; c) The FEFF program is available from: http://Feff.phys.washington.edu/feff.

Received: September 14, 2005
Published Online: February 9, 2006

  